Monitoring the Decomposition of Melamine in the Solid Phase by Electron Energy Loss Chronospectroscopy

Susana Trasobares,*,† Christine Kolczewski,‡ Riitta Räty,† Niclas Borglund,‡ Arianna Bassan,‡ Gilles Hug,§ Christian Colliex,† Stefan Csillag,‡ and Lars G. M. Pettersson‡

Laboratoire de Physique des Solides, UMR CNRS 8502, Building 510, Université Paris Sud 91405 Orsay, France, Department of Physics, Stockholm University, Stockholm Center for Physics, Astronomy and Biotechnology, SCFAB, S, 10691 Stockholm, Sweden, and ONERA−LEM, BP 72-29, Avenue de la Division Leclerc, 92322 Châtillon Cedex, France

Received: June 19, 2002; In Final Form: November 6, 2002

The decomposition process of melamine exposed to a high-energy electron beam has been investigated by monitoring the changes in the energy loss near edge structures (ELNES) using time-resolved electron energy loss spectroscopy. Calculations on different CN-containing molecules were performed in order to simulate the experimental ELNES observed at the different decomposition stages and to identify some of the intermediate compounds produced during this degradation process. As a result, we suggest that the amino groups are first eliminated as a release of N_2 gas. Then, the degradation of the molecule occurs through a reduction of the carbon−nitrogen double bonds. If the irradiation is maintained over longer periods, the formation of different CN fragments could then be possible.

1. Introduction

Using a semiempirical assumption based on a range of interesting hard materials, Liu and Cohen[1] predicted from ab initio calculations that the crystalline β-C_3N_4 compound should be stable and might have mechanical properties stronger than, or similar to, diamond. This has stimulated a lot of experimental efforts to synthesize and characterize carbon nitride materials. The production by different processing routes of CN_x films[2−5] and CN_x nanotubes[6−10] using several different techniques has been reported. All investigations generally show that only a limited amount of nitrogen may be inserted in the carbon network. Among the techniques applied so far, X-ray photoelectron spectroscopy (XPS) and electron energy loss spectroscopy (EELS) are interesting methods in that they, in the most favorable cases, allow us to obtain chemical compositions as well as information on the atomic structure and bonding of the materials. However, a correct identification of the nature of the bonding is difficult in amorphous materials where structural hypotheses are complicated as, for example, in amorphous CN materials. The interpretation of the near edge structure (NES) of the absorption edges is not trivial, and a close connection with theory becomes essential. Only transitions from 1s to π^* antibonding orbitals can easily be observed as sharp peaks several electron volts under the ionization edge. The position of such a peak is expected to be connected to different atomic configurations as, for example, in the case of sp- or sp^2-bonded carbon and nitrogen atoms. Thus, a precise characterization of these materials can be greatly facilitated by comparison with reference spectra of known materials or by comparison with reliably predicted NES from possible model structures. These spectra are used as fingerprints of the electronic structure of the material or molecule in order to establish which type of bonding is present. This will be used in the present work to identify the degradation products of melamine exposed to a high-energy electron beam.

Melamine (*s*-triazine-2,4,6-triamine, $C_3H_6N_6$), Figure 1a, has been used in the production of melamine-formaldehyde, resins for surface coating, laminates and adhesives, and in the production of flame retardants.[11] Recently, it has been used as an organic precursor in the production of CN_x nanotubes by pyrolysis[8,10] and detonative decomposition.[12]

The decomposition of melamine has been previously reported, and different mechanisms have been proposed. The formation of melam (molecular weight (MW) = 235, $C_6H_9N_{11}$) and melem (MW = 218, $C_6H_6N_{10}$), both with extended rings and elimination of NH_3 as a gas, has been observed by thermal decomposition of melamine.[13,14] Ju et al.[15] have studied the fragmentation of the melamine ring via electron impact ionization, laser desorption ionization, and collision-induced dissociation. They observed that bombarding with 70 eV electrons yielded mainly $CH_3N_2^+$ and $C_2H_4N_5^+$ apart from melamine ions. In addition, other molecular fragments, as well as NH_4^+, were observed in the mass spectroscopy data. It has been found that the higher the electron energy, the higher is the fraction of small fragments. As the electrons in the microscope have a kinetic energy about a thousand times higher than in the experiments of Ju et al.,[15] it could be presumed that molecules will indeed be fragmented.

We have found the melamine to be extremely sensitive to radiation damage by high-energy electrons during observation in a transmission electron microscope (TEM). This offers an interesting possibility to study its degradation decomposition process by following the changes in the carbon and nitrogen NES. In the current study, we present the use of the NES spectra at different stages of the decomposition of the melamine molecule to monitor changes in the bonding characteristics and composition in order to identify likely decomposition pathways

* To whom correspondence should be addressed. Argonne National Laboratory, 9700 S. Cass Ave., Material Science Division, Bldg. 200/D125, Argonne, IL 60439. E-mail: trasos@rpi.edu.
† Université Paris Sud 91405 Orsay.
‡ Stockholm Center for Physics, Astronomy and Biotechnology.
§ ONERA−LEM.

10.1021/jp026340j CCC: $25.00
Published on Web 12/13/2002

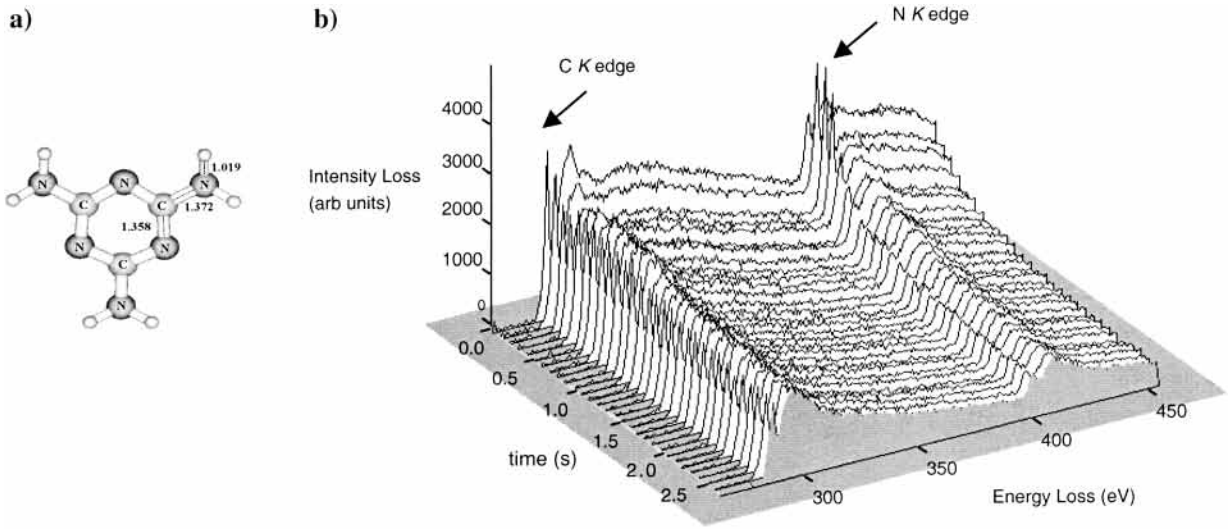

Figure 1. (a) Melamine molecule structure. b) A collection of 30 spectra; every spectrum is a sum of 10 consecutive spectra of identical ELNES, every one recorded with an acquisition time of 9 ms. It represents the first stages in the decomposition process of the melamine.

and to characterize the intermediate species involved at various stages during this process.

2. Experimental Procedure and Data Acquisition

Melamine powder (Aldrich, 99%+), Figure 1a, was ground with a mortar and suspended in acetone for TEM observation. The sample was analyzed in a VG 501 scanning transmission electron microscope (STEM) operating at 100 kV and equipped with a Gatan parallel EELS detector. The energy resolution of the whole system was about 0.7 eV. Recently, a specific charge-coupled device (CCD) camera was fitted to the spectrometer to improve the detection sensitivity.[16] With this new equipment, the required acquisition times for achieving a satisfactory signal-to-noise ratio in any spectrum are of the order of 5−10 ms for the plasmon region and 10 ms to 1 s for the core loss region. This short acquisition time permits us to investigate the transformation of the materials under the beam. The modifications in the NES during irradiation were studied by time-resolved EELS (chronospectroscopy): a probe of 0.5 nm diameter with a current of ca. 0.15−0.20 nA was fixed at a specific location of the specimen, and a series of spectra were recorded as a function of time or equivalently of the dose; the incident flux was typically 5×10^9 e^-/nm^2 s. The sample was found to be extremely radiation sensitive, and immediate visual changes could be seen in the image when the beam was focused on the sample. To detect the stages in the decomposition process, a bunch of 2000 spectra were recorded at intervals of 9 ms. Figure 1b shows a series of 30 such spectra. The characteristic signals corresponding to the C and N *K* edges have been monitored. We observed significant changes with time in the spectral features at both edges but in particular at the N *K* edge where, at the first stages of the process, the intensity of the sharp peak increased during a few milliseconds after which it started to decrease. During the exposure, we furthermore observed a strong reduction of the overall absorption indicative of significant loss of mass during the course of the experiment. Thus, the analysis was limited to the initial few seconds of exposure.

3. Computational Methods and Spectra Modelling

The density functional theory (DFT) calculations for the NES spectra were performed at the gradient-corrected DFT level using the deMon program.[17] The intensities were computed in the dipole approximation, which is valid for small momentum transfer in inner shell EELS.[18] The theoretical spectra were generated by the transition potential (TP) method[19,20] in combination with a double basis set technique.[21] A detailed description of the method and implementation within the DFT framework can be found in ref 22. Briefly, the orbitals for the molecule are determined using a good quality molecular basis set with a half-occupied core orbital at the ionization site. The orbitals for the excited electrons are then obtained by diagonalizing the Kohn−Sham matrix built from the density from the TP calculation; the basis set is in this second step extended with a large set of diffuse basis functions (∼150 functions) centered on the excited atom to describe Rydberg and continuum states. The obtained orbital energies and computed transition moments provide a representation of the excitation energies and associated intensities in the theoretical spectrum.

The TP calculation accounts for most of the relaxation effect upon core ionization and provides a single set of orthogonal orbitals for the spectrum calculation. To determine the absolute energy position of the spectrum, we performed ΔKohn−Sham (ΔKS) calculations of the ionization energy (IP), using the fully ionized core hole state. Relativistic effects on the IP of 0.3 eV for the N edge and 0.2 eV for the C edge[23] were added to give the overall shift of the spectrum. In the ΔKS calculations, the noncore-excited C (N) atoms were described by effective core potentials (ECP).[24] This simplifies the definition of the core hole state, since the use of an ECP description eliminates the 1s level of the atom to which it is applied. The ECP's introduce insignificant effects (<0.1 eV) on the computed spectrum.

The DFT TP calculation of the spectrum assumes a frozen molecular ion density and thus neglects the relaxation effects on the molecular ion core upon adding the excited electron. This effect is largest for the valencelike π^* excitations, and these states were therefore computed with fully relaxed ΔKS calculations. For triazine, pyrrole, and pyridine, a sequence of the most prominent excitations, which are transitions into antibonding orbitals of σ symmetry and Rydberg orbitals, was furthermore calculated in fully relaxed ΔKS excited state calculations. It was found that the first transitions show relaxation effects around 2.0−2.5 eV, whereas higher transitions with a lesser amount of valence orbital mixing usually show relaxation shifts in the order of the shift of the ionization potential (around 1.5 eV).

For details, see ref 25. For these three molecules, the corresponding peaks in the energy-shifted TP spectrum have been shifted to include the additional relaxation effects obtained from the specific ΔKS excited state calculations, whereas for the remaining molecules only the first π^* transition was shifted according to the calculated relaxation. The other prominent transitions were shifted, depending on their orbital character, by the same amount as the first π^* resonance (valencelike) or according to the ionization potential (Rydberg character).

As a first step, for each molecule, a geometry optimization was performed using a triple-ζ valence plus polarization (TZVP) basis[26] in a [4s, 3p] contraction with one added d function for nitrogen and carbon and a primitive (5s) basis set augmented with one p function and contracted to [3s, 1p] for hydrogen.[27] To obtain an improved representation of relaxation effects in the inner orbitals, the ionized center was described by the IGLO-II basis of Kutzelnigg et al.[28] In the spectrum calculations, a large [19s, 19p, 19d] diffuse even-tempered basis set centered on the ionization site was added; it was employed only in the last step of the calculation. The spectrum was generated by a Gaussian convolution of the discrete spectrum with a broadening in the preedge region that was selected to resemble the experimental resolution. For the synchrotron reference spectra, we thus used 0.7 eV full width at half-maximum (fwhm) for the features before the edge, while for the EELS data Gaussians with fwhm 1.5 eV were used. The continuum states were convoluted using Gaussians with a fwhm that was linearly increased over an interval of around 10 eV from the edge up to a fwhm of 3.5 eV. At higher energies, the fwhm was kept constant at this value. All DFT calculations were performed using the gradient-corrected Perdew[29] exchange and correlation functionals.

4. Interpretation and Discussion

4.a. Dose Dependence of the Mass Losses and Changes in Atomic Ratios. To study the NES, spectra t_1-t_3, representing the different transformation stages as seen in the carbon and nitrogen *K* edges, are displayed in Figure 2a. Each spectrum is the sum of 20 consecutive spectra with rather identical NES. The spectra t_1, t_2, and t_3 were recorded after irradiating the melamine for 0.4, 2.7, and 4.4 s, respectively. No significant changes are observed beyond a typical time of 5 s. To study the limiting cases (initial and infinite state), the NES was recorded as soon as the beam was focused on the sample ($t = 0$, melamine spectrum in Figure 2b) and after irradiating the sample with the electron beam for 140 s with an acquisition time of 800 ms (spectrum t_{140}). To record a spectrum after 140 s of electron irradiation was not possible in the present experiment because of strong carbon contamination. Spectrum t_3* was obtained as a combination of spectrum t_3, Figure 2a, and an amorphous carbon spectrum (34% of amorphous C is being added to the spectrum t_3), and it reflects the carbon contamination artifact. Therefore, in the present experiment, t_{140} is considered the infinite state t_∞.

The spectra labeled t_1, t_2, and t_3, as well as the "pure" melamine spectrum, all present a strong π^* peak at the carbon edge. The shape of the C *K* and N *K* edges in the melamine and the t_1 spectra is characteristic of thick samples, since they exhibit an additional contribution at 310 and 420 eV, respectively; i.e., an energy equal to the edge threshold plus the plasmon resonance energy. These additional features, due to multiple losses in thick samples, are not observed in spectra t_2 and t_3, which is evidence for significantly thinner samples in these cases.

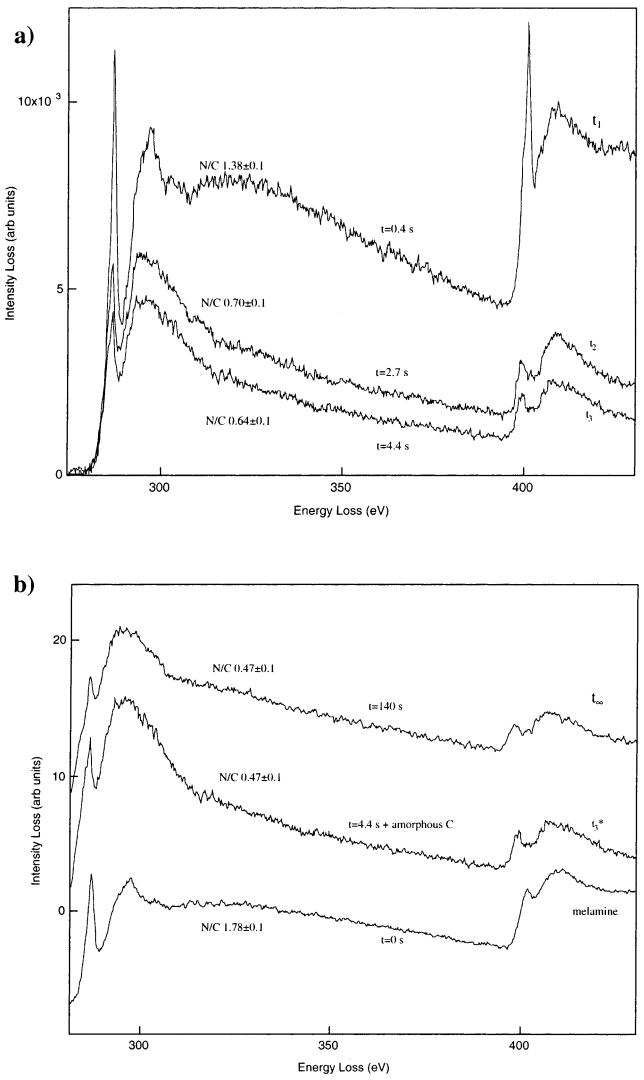

Figure 2. Spectra corresponding to different stages in the melamine decomposition process. (a) t_1, t_2, and t_3 spectra were recorded after 0.4, 2.7, and 4.4 s of electron beam irradiation, respectively. (b) NES observed at the initial state of the process ("melamine") and after 140 s of electron beam irradiation (t_∞). Spectrum t_3* shows the effect of adding 34% of amorphous carbon to the t_3 spectrum of panel a.

The composition ([N]/[C] at ratio) was measured from the EELS data by determining the integrated intensity of the C and N *K* edges after background subtraction. A classical power law ($A\,E^{-r}$) of the background and a hydrogenic model for the *K* edge cross-sections have been used.[30] A continuous reduction of the intensity at both the C and the N edges is found during the irradiation process but with a much more rapid initial nitrogen loss as indicated in Figure 3. The hydrogen content cannot be directly quantified. The figure also shows the integrated intensity of the background before the C *K* edge, I_b, which we assume to be proportional to the local mass thickness.[31] In the specific case considered here, this background is essentially due to the very high-energy tail of the collective and individual electronic excitations and should reflect the local electron density contributed by carbon, nitrogen, and hydrogen. Estimates of the thickness variations between t_1, t_2 and t_2, t_3 using the background intensity obtained from the EELS spectra give reductions of thickness of 55 and 24%, respectively. The local thickness then increases again as evident from the increase of the signal in the 320−330 eV region in the t_∞ spectrum. This is most likely due to amorphous carbon

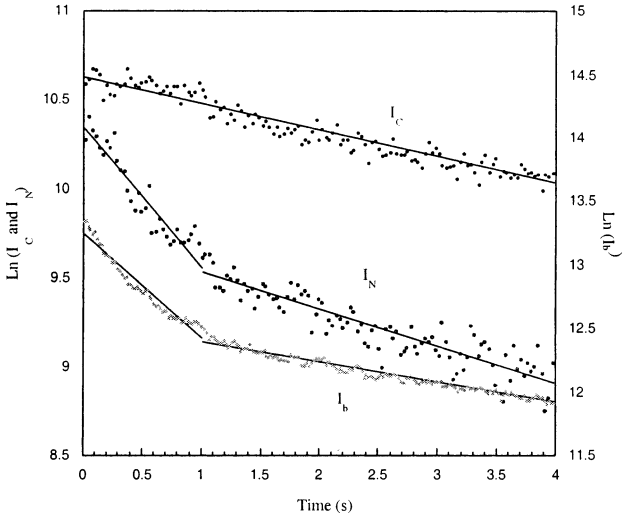

Figure 3. Logarithmic variation of the carbon and nitrogen intensities I_C, I_N (left axis), and background intensity, I_b (right axis).[32]

contamination, which cannot be avoided on the specimen during the process.

To obtain some initial insight into the decomposition process, we may compare the background intensity variation (I_b) with those specific for carbon (I_C) and nitrogen (I_N). The nitrogen loss first follows an exponential law with a short characteristic time before decreasing more slowly after about 1 s. This suggests that there is a rapid loss of nitrogen at the beginning of the process. To study the rate of decrease of N and of mass loss, a logarithmic analysis of the background intensity before the C *K* edge and of the carbon and nitrogen intensities, I_C and I_N, is presented in Figure 3. Both the background and the nitrogen, I_b and I_N, curves exhibit rather similar behavior with two different slopes;[32] the steeper one (~0.8) is typically valid over the first second while the slope for longer exposures (0.2) is closer to the slope characteristic for the carbon removal loss over the whole investigated time scale (i.e., up to a dose of about 25×10^9 e^-/nm^2). Considering that the amino groups of the melamine are only connected with single bonds to the framework of the molecule, it seems probable that these groups, rather than the multiply connected ring atoms, are affected through hydrogen loss or bond cleavage as a result of the excitation and deexcitation processes. The details of this process will be discussed further below.

4.b. Test of the Validity of the Modeling: Comparison with Experimental Spectra on Reference Molecules. The NES at the *K* edges correspond to transitions from 1s states to unoccupied states above the Fermi level and the structure in the NES will thus reflect the local bonding.[18] Therefore, it is interesting to compare the NES at the N *K* edge in the recorded spectra to corresponding data in CN molecular systems such as triazine[33] ($C_3H_3N_3$), pyridine[34] (C_5H_5N), and pyrrole[35] (C_4H_5N) (Figure 4); these will also be used for testing the validity of our computational approach.

All of these compounds are based on aromatic molecules in which the nitrogen atoms are present in sp^2 hybridization but where the N can still contribute differently to the molecular orbital structure. The fifth valence electron of the N atom can form a lone pair either with the remaining unhybridized $2p_z$ orbital or with one of the sp^2 orbitals. The first case leads to a localized $2p_z$ lone pair, and the three sp^2 hybrid orbitals bond to other atoms. This case is observed in the pyrrole molecule. If the fifth electron instead forms a lone pair with one of the

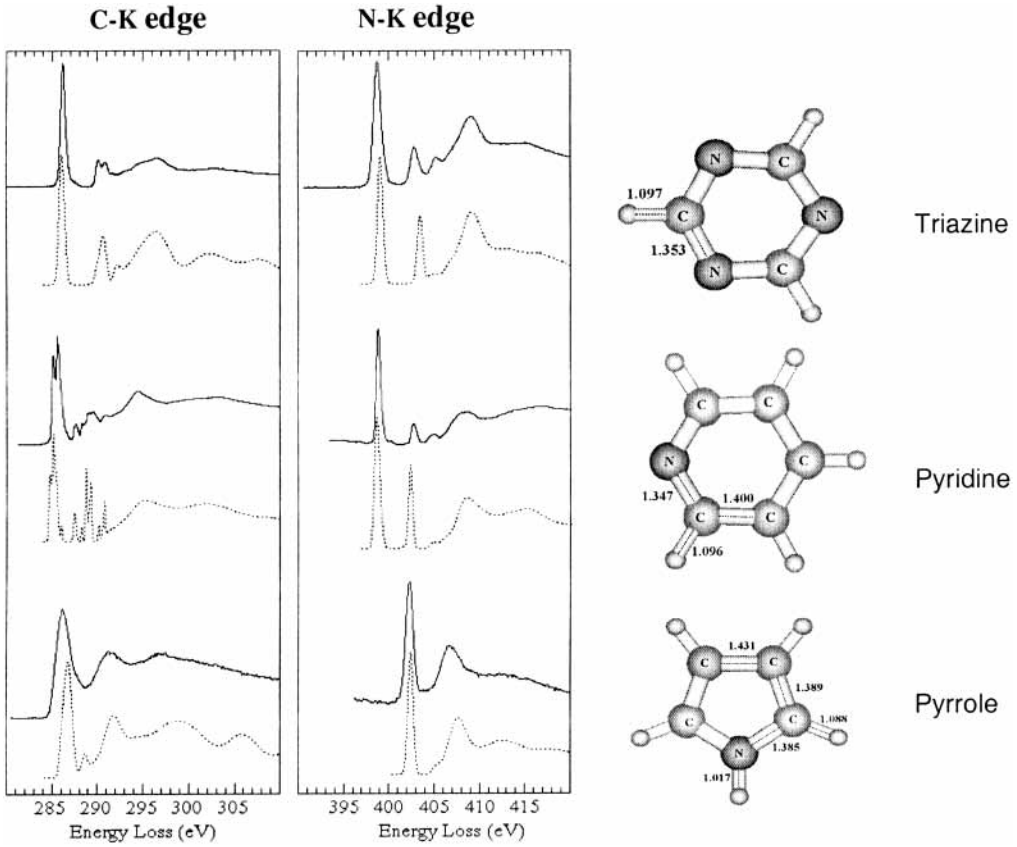

Figure 4. Experimental (solid lines) and computed (dotted lines) C, N *K* edge spectra and structures for the molecules triazine, pyridine, and pyrrole. The experimental data were obtained from the Hitchcock (http:/xray.uu.se/hypertext/corexdb.html) database. The bond distances are in angstroms.

sp^2 hybrid orbitals, the atom is left with two sp^2 hybrid orbitals and one unfilled $2p_z$ and can therefore form one π and two σ bonds as observed in the pyridine molecule. However, in the pyridine case, even though the N atom exhibits sp^2 hybridization, it does not contribute any mobile electron to the structure. Nitrogen is more electronegative than carbon and the nitrogen thus attracts electrons from the rest of the molecule, leading to an enhanced C *K* edge π^* peak, which is found at 286.2 eV for *s*-triazine (286.1 eV), with the computed values in parentheses. The π^* peak becomes broader in the case of pyrrole and pyridine, and is found at 286.3 eV (286.4 eV) and at 284.9 eV (284.7 eV), respectively. The origin of the broadening in the π^* peak is due to the different chemical shifts on the carbons induced by the presence of the nitrogen in the ring.[25,36]

The situation is more complex for the nitrogen edge. The first peak at the N *K* edge at 398.4 eV in pyridine and at 399.0 eV in triazine displays similarities in shape and energy position for pyridine and triazine. This peak is associated with transitions from 1s core states to unoccupied molecular states of π^* symmetry (π^* peak). For pyrrole, this transition is shifted up in energy and is observed at 402.3 eV (402.4 eV); the sharp feature contains contributions both from the π^* (dominating contribution) and some σ^* contribution at the same energy (at 0.5 eV higher energy in the TP calculation).

The agreement between the computed and the experimental reference spectra is very good, for both the energy positions and the relative intensities but most importantly for the overall appearance of the computed spectra, which gives credibility to the computational approach: given a specific molecular structure and environment, we can very accurately predict the NES features theoretically.

4.c. Possible Intermediates in the Decomposition Process. We now turn to a discussion of the experimental spectra of melamine at the different stages in the electron beam-induced decomposition as shown in Figure 2. Starting with the C *K* edge of the melamine spectrum, we identify a strong π^* peak at 287.3 eV and a σ^* peak at 297.8 eV. The value for the π^* peak is higher than those observed for the reference CN molecules, but the position and shape of the σ^* peak are similar to that of triazine. The shift in the π^* position, relative to, e.g., triazine, is confirmed in the present theoretical calculations and is due to the presence of the additional electron-donating amino groups bonded to each carbon atom in the melamine molecule. The N *K* edge in the melamine spectrum shows a peak at 400.5 eV, which is the energy position typical of molecules such as ammonia (NH_3) and methylamine (CH_3NH_2)[2]. The σ^* position at about 9 eV higher energy is consistent with the separation found from the carbon spectrum. However, we must point out that even at $t = 0$, the N/C ratio is somewhat lower than expected for the pure melamine molecule (1.78 ± 0.1 vs 2.0).

In spectrum t_1, the C *K* edge presents the same structure as observed for melamine, which suggests that the C aromatic structure of the molecule is not affected; that is, the integrated intensity under the C π^* peak at 287 eV is very similar to that of melamine. On the other hand, the N *K* edge already shows significant differences, which is not surprising because a reduction of the N/C ratio from 1.78 to 1.38 (a lower value than what would be expected for the melam or melem molecules) is measured. An additional sharp and dominant peak is observed at 401.1 and is attributed to the $1s \rightarrow \pi^*$ excitation for N_2 gas.[37,38] The absence of changes in the C *K* edge structure, the presence of the peak at 401.1 eV, and the decrease of the N content suggest that the amino groups are first eliminated, accompanied by formation and elimination of N_2 as one product during the first stage.

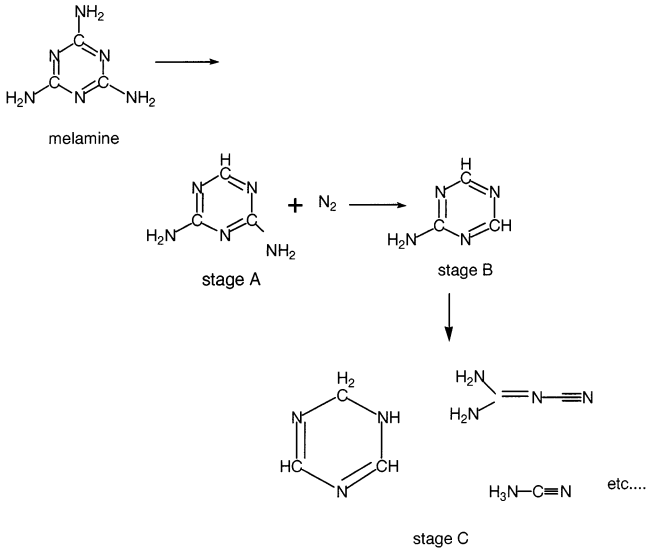

Figure 5. Proposed mechanism for the first stages of the decomposition of melamine.

In spectrum t_2, the π^* peak at the C *K* edge still does not change significantly apart from a small decrease in the intensity, but some clear modifications of the σ shape are observed. Changes in the N *K* edge are more important during this stage of the process. Comparing the t_1 and t_2 experimental spectra, we notice that the intensity of the peak at 401.1 eV (N_2 gas peak) strongly decreases while two new peaks appear at 398.9 and 401.9 eV in the nitrogen spectrum. At that time, the thickness of the specimen has also decreased by 55%. The nitrogen content in the sample decreases from 1.38 to 0.70 N/C (t_2) and to 0.64 (t_3) accompanied by an increase in the relative intensity of the 398.9 eV peak. This peak is also observed in the *s*-triazine molecule; however, the 401.9 eV peak is observed at higher energy than the corresponding excitation in the triazine case. These observations confirm that the loss of nitrogen in the first stage of decomposition involving the desorption of N_2 molecules could be due to the loss of the amino groups, which therefore does not influence the aromaticity of the molecule.

Spectrum t_∞ (N/C ratio of only 0.47) was recorded from a melamine solid after 140 s of electron beam irradiation. The low N/C value can be due to a combination of loss of nitrogen in the decomposition process and accumulation of carbon by contamination in the microscope. The π^* peak at the C *K* edge at t_∞ is weaker than in the t_1 and $t_{2,3}$ spectra, which indeed indicates that the ratio of sp^2 to sp^3 carbon is decreasing. The first nitrogen peak at the t_∞ spectrum of Figure 6b, on the other hand, is getting broader, exhibiting a shape, which is quite common in CN thin films. It presents a shoulderlike feature, which most likely originates from contributions from various nitrogen-bonding configurations.

In Figure 5, a scheme of the possible stages present in the decomposition process of melamine is displayed. The spectra from the different stages have been computed and compared to the experimental results, as described in the next section.

5. Identification of Some Decomposition Intermediates by Comparison of Measured and Calculated ELNES Profiles

In this section, we present our computed spectra for a number of possible intermediate decomposition products. The overall accuracy of our approach has been discussed in Section 4.b

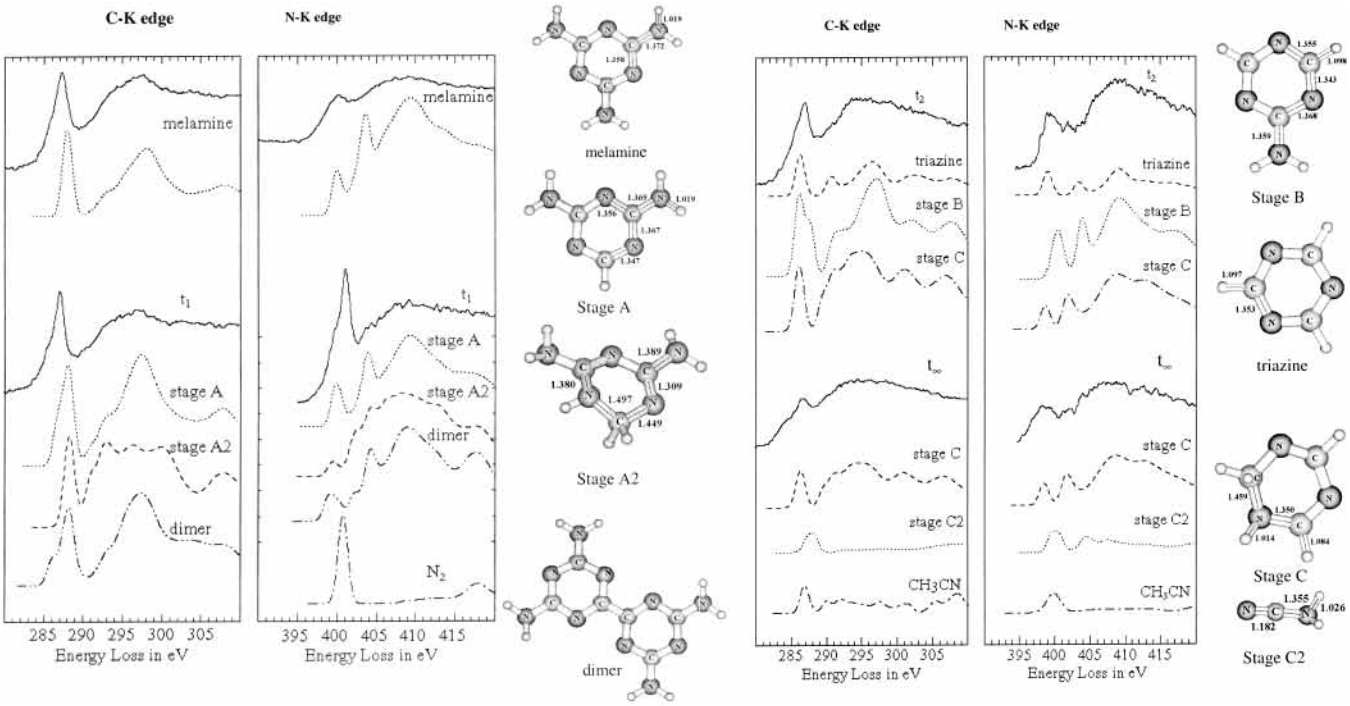

Figure 6. (a) Experimental (solid line) and computed ELNES at the first decomposition state. The molecular structures are also displayed with the bond distances in angstroms. (b) Experimental (solid line) and computed ELNES of the t_2 and t decomposition stages. The molecular structures are also displayed with the bond distances in angstroms.

above where we found a quite good agreement for the set of calibration molecules. A comparison between experimental and calculated spectra can then be used to identify some of the intermediate molecular species likely to be involved in the process. As a result of this comparison, the mechanism summarized in Figure 5 can be proposed.

It should be noted that the calculations have been performed for the isolated molecules such that possible effects due to the presence of the solid surrounding are not included. These effects should mainly contribute via a general broadening of the individual molecular spectrum as well as quenching of the higher Rydberg states. Application of a larger broadening to the computed transitions could to some extent mimic this effect but would remove information on the underlying contributions.

A study of the spectrum variations shows the different stages of the decomposition process as follows: Starting with the initial melamine spectrum, we find a good agreement between the computed and the measured spectra for the C *K* edge (Figure 6a). However, differences are observed in the nitrogen spectrum. The calculations show that the nitrogen spectrum should contain contributions from both the ring atoms and the amino groups, where the ring atoms give the main contribution to the π^* resonance at 400.1 eV (computed), while the amino groups dominate the peak at 404 eV. The relative intensities in these regions can thus be used to follow the removal of amino groups from the melamine. In the experimental spectrum, the peak at 404 eV is not resolved, but significant intensity is observed in this energy region. To explain this discrepancy, we can refer to the fact that these groups are those likely modified by the solid nature of the specimen. The π^* resonance is a valence excitation, while the excitation at 404 eV on the more exposed amino groups has more Rydberg character. It is also important to recall that the experimental spectrum, called melamine, has a lower N content than expected for the melamine molecule and the radiation-induced melamine decomposition is thus probably already initiated in the spectrum at $t = 0$. These arguments could explain the differences observed in the σ part of the N *K* edge in the melamine spectrum.

During the first stages of the decomposition process, a decrease of nitrogen content (i.e., with N/C from 1.78 to 1.38), combined with the appearance of a shoulder at the C *K* edge, is observed, as can be seen in spectrum t_1. It suggests that the eliminated N comes from the external amino groups of the melamine molecule, which do not affect the aromatic structure of the molecule (Figures 5 and 6a, stage A, *s*-triazine-2,6-diamine). This is consistent with the computed spectrum where the carbon without the amino group (stage A) is chemically shifted to 1.3 eV lower energy, whereas the two carbons connected to an amino group are unchanged in energy position as compared to the melamine. This results in an intensity ratio of 1:2 for the shoulder to the main peak in the C *K* edge t_1 spectrum; this is also observed experimentally and is consistent with an average initial loss of one amino group per melamine molecule. The same result for the carbon edge is obtained for the dimerized melamine, where we assume elimination of one amino group from each of two neighboring molecules and a subsequent bond formation between them. This situation is indistinguishable spectroscopically from the simple loss of an amino group. We can thus not exclude polymerization products as a result of the exposure.

During the first 90 ms of the process, an increase in intensity of the 401.1 eV peak at the N *K* edge is observed. Then, the intensity starts decreasing until its disappearance after 1.2 s. The position of this peak (401.1 eV) corresponds to the strong π^* excitation in N_2 gas[38] and is absent in all of the investigated intermediates except for N_2 as seen from Figure 2. The peak at 399.7 eV (computed) corresponds to the essentially unperturbed π^* of the ring; this now shows a higher intensity than the peak at 404 eV associated with the amino group. A small contribution from the stage A2 molecule (*s*-triazine, 2,4-diamino-1,6-dihydro, the structure is displayed in the inset in Figure 6) could also be present as well as polymerized products. However, we can

conclude that at the first stage of melamine decomposition, the formation (increase in intensity) and elimination (decrease in intensity of the 401.1 eV peak) of N_2 gas are involved, although other volatile nitrogen-containing decomposition products, as observed by Ju et al.,[15] cannot be excluded. The loss of nitrogen occurs mainly from the amino groups connected to the ring.

As the amino groups are successively eliminated from the melamine molecule, the relative intensity of the contributions from the two different carbons shift such that the peak at lower energy becomes dominating. For the stage A molecule where one amino group had been lost, the π^* excitation from this carbon was found at 1.3 eV lower energy (corresponding to triazine) and the intensity ratio was 1:2. For the stage B molecule (*s*-triazine-2-amino) with only one carbon connected to an amino group, the lower energy peak becomes dominant with the expected 2:1 ratio.

For the N *K* edge, a corresponding reduction of the intensity of the second (amino) peak is expected and the intensity in this region is indeed strongly reduced as compared with spectrum t_1. In addition, two π^* peaks at the N *K* edge at 398.9 and 401.9 eV are resolved in the spectrum. The position of these peaks is similar to what is observed for the triazine molecule and polymerized products as well as for stages B and C (*s*-triazine, 1,2-dihydro), which thus are possible intermediates. Stage C models the loss of aromaticity seen in the spectrum as due to addition of hydrogen from the decomposed amino groups. The presence of additional fragments in combination with initial stages of amorphous carbon deposition could account for the measured N/C ratio lower than 1 in the spectrum.

The last observed stage, spectrum t_∞, shows a strong decrease in the intensity of the π^* peak at the C *K* edge, which suggests that the ratio of sp^2 to sp^3 carbon is reduced. This can be due to a combination of amorphous carbon deposition, and that the aromatic character of the ring is affected. The overall N/C ratio (0.64 ± 0.1) is only about half of that of the triazine ring (N/C $= 1$), which suggests some deposited amorphous carbon. The N *K* edge presents features such as what is observed when different N contributions are present, i.e., the peaks at 398 and 401 eV as represented by, e.g., stage C. This stage suggests that a reduction of the carbon−nitrogen double bonds is taking place either through addition of hydrogen (computed stage C) or through fragmentation (computed stage C2, N−cyanoamine). The theoretical ELNES suggests that the spectrum t_3 has contributions from at least two components, e.g., stages C2 and C. No further stages could be observed during the experiment.

The ELNES of molecules, such as CH_3CN, with higher C content have been simulated in order to explain the low N content in the sample. However, the calculated spectrum (Figure 6b) can only suggest that some of the low-energy prepeaks on both the C and the N *K* edges can incorporate contribution from smaller fragments.

6. Conclusions

The decomposition process of melamine exposed to a high-energy electron beam has been investigated by monitoring the changes in the ELNES using time-resolved EELS. Calculations performed at the gradient-corrected DFT level using the deMon program were used to simulate the experimental ELNES observed at the different decomposition stages and to identify the different intermediate compounds produced during this degradation process. The computational procedure was validated on a set of model molecules and then applied to the proposed intermediates. The present study shows a rather satisfactory agreement between simulated spectra resulting from a mixing of simulated ELNES of different CN-containing molecules and experimental ELNES, and the observed differences can generally be accounted for. From this comparison, we suggest that the amino groups are first eliminated leading to a release of N_2 gas. Then, the degradation of the molecule occurs through a reduction of the carbon−nitrogen double bonds in the triazine ring. If the irradiation is maintained over longer periods, the formation of different CN fragments and polymerization products could be possible, but it is generally masked by the contamination effects involving supply of amorphous carbon. This study has also demonstrated the new capacity of time-resolved EELS analysis for monitoring in situ dynamic processes involving chemical and electronic changes.

Acknowledgment. M. Tencé and W. K. Hsu are thanked for help with experiments, and S.T. and R.R. thank K. Kordatos for useful discussions about the decomposition mechanism. The financial support of the EU-TMR network Synthesis, Structure, and Properties of New Carbon-Based Hard Materials and of the Swedish Foundation for Strategic Research is gratefully acknowledged.

References and Notes

(1) Liu, A. Y.; Cohen, M. L. *Science* **1989**, *245*, 841−842.
(2) Wang, Y. L.; Mebel, A. M.; Wu, C. J.; Chen, Y. T.; Lin, C. E.; Jiang, J. C. *J. Chem. Soc., Faraday Trans.* **1997**, *93*, 3445−3451.
(3) He, D. W.; Zhang, F. X.; Zhang, X. Y.; Qin, Z. C.; Zhan, M.; Liu, R. P.; Xu, Y. F.; Wang, W. K. *J. Mater. Res.* **1998**, *13*, 3458−3462.
(4) Muhl, S.; Mendez, J. M. *Diamond Relat. Mater.* **1999**, *8*, 1809−1830.
(5) Montigaud, H.; Tanguy, B.; Demazeau, G.; Alves, I.; Birot, M.; Dunogues, J. *Nitrides and Oxynitrides*; 2000; Vol. 325-3, pp 31−36.
(6) Sen, R.; Satishkumar, B. C.; Govindaraj, A.; Harikumar, K. R.; Raina, G.; Zhang, J. P.; Cheetham, A. K.; Rao, C. N. R. *Chem. Phys. Lett.* **1998**, *287*, 671−676.
(7) Sung, S. L.; Tsai, S. H.; Tseng, C. H.; Chiang, F. K.; Liu, X. W.; Shih, H. C. *Appl. Phys. Lett.* **1999**, *74*, 197−199.
(8) Grobert, N.; Terrones, M.; Trasobares, S.; Kordatos, K.; Terrones, H.; Olivares, J.; Zhang, J. P.; Redlich, P.; Hsu, W. K.; Reeves, C. L.; Wallis, D. J.; Zhu, Y. Q.; Hare, J. P.; Pidduck, A. J.; Kroto, H. W.; Walton, D. R. M. *Appl. Phys. A* **2000**, *70*, 175−183.
(9) Suenaga, K.; Yudasaka, M.; Colliex, C.; Iijima, S. *Chem. Phys. Lett.* **2000**, *316*, 365−372.
(10) Trasobares, S.; Stéphan, O.; Colliex, C.; Hsu, W. K.; Kroto, H. W.; Walton, D. R. M. *J. Chem. Phys.* **2002**, *116*, 8966−8972.
(11) Vandershall, H. L. J. *Fire Flam.* **1971**, *2*, 97.
(12) Kroke, E.; Schwarz, M.; Buschmann, V.; Miehe, G.; Fuess, H.; Riedel, R. *Adv. Mater.* **1999**, *11*, 158−161.
(13) Costa, L. C. G. *J. Therm. Anal.* **1988**, *34*, 423−429.
(14) Ono, S.; Funato, T.; Inoue, Y.; Munechika, T.; Yoshimura, T.; Morita, H.; Rengakuji, S. I.; Shimasaki, C. *J. Chromatogr. A* **1998**, *815*, 197−204.
(15) Ju, S.; Han, C.; Wu, C.; Mebel, M.; Chen, Y. *J. Phys. Chem. B* **1999**, *103*, 582−596.
(16) Ballongue, P.; Tencé, M. Presented to JEELS 99-Autrans, 1999.
(17) Casida, M. E.; Daul, C.; Goursot, A.; Hermann, K.; Koester, A.; Pettersson, L. G. M.; Proynov, E.; St-Amant, A.; Sala-hub, D. R.; Carravetta, V.; Duarte, H.; Godbout, N.; Guan, J.; Jamorski, C.; Leboeuf, M.; Malkin, V.; Malkina, O.; Nyberg, M.; Pedocchi, L.; Sim, F.; Triguero, L.; Vela, A. *deMon-KS StoBe*, version 1.0.; deMon Software, 2001.
(18) Stöhr, J. *NEXAFS Spectroscopy*; Springer-Verlag: Berlin, Heidelberg, 1996.
(19) Slater, J. C. *Adv. Quantum Chem.* **1972**, *6*.
(20) Slater, J. C.; Johnson, K. H. *Phys. Rev. B* **1972**, *5*, 844.
(21) Ågren, H.; Carravetta, V.; Vahtras, O.; Pettersson, L. G. M. *Theor. Chem. Acc.* **1997**, *97*.
(22) Triguero, L.; Pettersson, L. G. M.; Ågren, H. *Phys. Rev. B* **1999**, *58*, 8097.
(23) Triguero, L.; Plashkevych, O.; Pettersson, L. G. M.; Ågren, H. *J. Electron Spectrosc. Relat. Phenom.* **1999**, *104*, 195.
(24) Pettersson, L. G. M.; Wahlgren, U.; Gropen, O. *Chem. Phys.* **1983**, *80*, 7.
(25) Kolczewski, C.; Püttner, R.; Plashkevych, O.; Ågren, H.; Staemmler, V.; Martins, M.; Snell, G.; Schlachter, A. S.; Santánna, M.; Kaindl, G.; Pettersson, L. G. M. *J. Chem. Phys.* **2001**, *115*, 6426−6437.
(26) Dunning, T. H. *J. Chem. Phys.* **1971**, *55*, 716.

(27) Huzinaga, S. *J. Chem. Phys.* **1977**, *66*, 4245.
(28) Kutzelnigg, W.; Fleischer, U.; Schindler, M. *NMR−Basic Principles and Progress*; Springer-Verlag: Heidelberg, 1990.
(29) Perdew, J. P. *Phys. Rev. B* **1986**, *33*, 8822.
(30) Leapman, R. D.; Rez, P.; Mayers, D. F. *J. Chem. Phys.* **1980**, *72*, 1232.
(31) Reimer, L. *Scanning Electron Microscopy*, *Physics of Image Formation and Microanalysis*; Springer-Verlag: Berlin, Heidelberg, 1985.
(32) The linear fitting parameters for Figure 3 are the following; r is the regression coefficient: ($t = 0-1$ s) Ln $I_b = 13.24-0.82t$, $r = 0.95$, Ln $I_N = 10.34-0.78t$, $r = 0.98$; ($t = 1-5$ s) Ln $I_b = 12.55-0.16t$, $r = 0.98$, Ln $I_N = 9.74-0.21t$, $r = 0.91$; ($t = 0-5$ s) Ln $I_C = 10.63-0.15t$, $r = 0.96$.
(33) Apen, E.; Hitchcock, A. P.; Gland, J. L. *J. Phys. Chem.* **1993**, *97*, 6859−6866.
(34) Horsley, J. A.; Stöhr, J.; Hitchcock, A. P.; Newbury, D. C.; Johnson, A. L.; Sette, F. *J. Chem. Phys.* **1985**, *83*, 6099−6107.
(35) Newbury, D. C.; Ishii, I.; Hitchcock, A. P. *Can. J. Chem. Rev. Can. Chim.* **1986**, *64*, 1145−1155.
(36) Hannay, C.; Duflot, D.; Flament, J. P.; Hubin-Franskin, M. J. *J. Chem. Phys.* **1999**, *110*, 5600.
(37) McLaren, R.; Clark, S. A. C.; Ishii, I.; Hitchcock, A. P. *Phys. Rev. A* **1987**, *36*, 1683−1701.
(38) Trasobares, S.; Stéphan, O.; Colliex, C.; Hug, G.; Hsu, W. K.; Kroto, H. W.; Walton, D. R. M. *Eur. Phys. J. B* **2001**, *22*, 117−122.